Probabilistic Analytical Target Cascading using Kernel Density Estimation for Accurate Uncertainty Propagation

Yongsu Jung

Department of Mechanical Engineering, Korea Advanced Institute of Science and Technology,

Daejeon, 34141, South Korea

Jongmin Lee

Department of Mechanical Engineering, Korea Advanced Institute of Science and Technology,

Daejeon, 34141, South Korea

Mingyu Lee

Department of Mechanical Engineering, Korea Advanced Institute of Science and Technology,

Daejeon, 34141, South Korea

Namwoo Kang*

Department of Mechanical Systems Engineering, Sookmyung Women's University,

Seoul, 04310, South Korea

Ikjin Lee*

Department of Mechanical Engineering, Korea Advanced Institute of Science and Technology,

Daejeon, 34141, South Korea

Keywords: Multidisciplinary Design Optimization (MDO), Reliability-based Design Optimization (RBDO), Probabilistic Analytical Target Cascading (PATC), Uncertainty Propagation, Kernel Density Estimation (KDE)

*Co-corresponding author: nwkang@sookmyung.ac.kr (N. Kang), ikjin.lee@kaist.ac.kr (I. Lee)

Abstract

Probabilistic analytical target cascading (PATC) has been developed to incorporate uncertainty of random variables in a hierarchical multilevel system using the framework of ATC. In the decomposed ATC structure, consistency between linked subsystems has to be guaranteed through individual subsystem optimizations employing special coordination strategies such as augmented Lagrangian coordination (ALC). However, the consistency in PATC has to be attained exploiting uncertainty quantification and propagation of interrelated linking variables that are the major concern of PATC and other uncertainty-based multidisciplinary design optimization (UMDO). In previous studies, the consistency of linking variables is assured by matching statistical moments under the normality assumption. However, it can induce significant error when the linking variable to be quantified is highly nonlinear and non-normal. In addition, reliability estimated from statistical moments may be inaccurate in each optimization of the subsystem. To tackle the challenges, we propose the sampling-based PATC using multivariate kernel density estimation (KDE). The framework of reliability-based design optimization (RBDO) using sampling methods is adopted in individual optimizations of subsystems in the presence of uncertainty. The uncertainty quantification of linking variables equivalent to intermediate random responses can be achieved by multivariate KDE to account for correlation between linking variables. The constructed KDE based on finite samples of the linking variables can provide accurate statistical representations to linked subsystems and thus be utilized as probability density function (PDF) of linking variables in individual sampling-based RBDOs. Stochastic sensitivity analysis with respect to multivariate KDE is further developed to provide an accurate sensitivity of reliability during the RBDO. The proposed sampling-based PATC using KDE facilitates efficient and accurate procedures to obtain a system optimum in PATC, and the mathematical examples and roof assembly optimization using finite element analysis (FEA) are used to demonstrate the effectiveness of the proposed approach.

1. Introduction

Generally, a large-scale complex system such as a vehicle and an airplane consists of multiple and hierarchical subsystems which are intricately linked with each other through variables and responses making it challenging to optimize the whole system at once due to its complexity and dimensionality. Therefore, decomposition-based optimization methods with special coordination between linked subsystems have been developed to optimize the large-scale complex system (Alexandrov and Lewis 2002; Kokkolaras et al. 2004; Allison et al. 2009; Martins and Lambe 2013; Bayrak et al. 2016; Cho et al. 2016; Papalambros and Wilde 2017).

Analytical target cascading (ATC) is one of the decomposition-based methods where a system is partitioned into several hierarchical subsystems with targets and responses (Kim et al. 2003, 2006; Michelena et al. 2003; Tosserams et al. 2006, 2008; Han and Papalambros 2010; Kang et al. 2014a, b; Jung et al. 2018). In the early stage, ATC was originally specialized in hierarchical decomposition with multilevel subsystems, but non-hierarchical decomposition was proposed as well (Tosserams et al. 2010). However, these researches were established on deterministic conditions and thus may not find solutions for actual engineering applications influenced by various uncertainties. Therefore, it is necessary to take into account uncertainties propagated from subsystems, and uncertainty-based multidisciplinary design optimization (UMDO) was extensively reviewed in the literature (Yao et al. 2011). Probabilistic analytical target cascading (PATC) has been developed to treat the uncertainties in the framework of ATC (Kokkolaras et al. 2006; Liu et al. 2006; Xiong et al. 2010). Especially, PATC using moment-matching allows treating the consistency of interrelated probabilistic characteristics (i.e., linking variable) and the probabilistic constraints using statistical moments. This approach is intuitive and straightforward but can cause a significant error when the propagated distribution is highly non-normal resulting in an unreliable system optimum. Even if any parametric distribution is selected instead of the normal distribution, it has to be predetermined that is a major weakness of moment-matching since inappropriate distribution could be assumed and the random response of linking variables may not follow parametric distribution. On the other hand, Ouyang et al. (2014) proposed sequential PATC (SPATC) which combines sequential optimization and reliability

assessment (SORA) and PATC to improve its efficiency by decoupling the triple nested loop in PATC, and extended it to deal with mixed uncertainty including interval variables (Ouyang et al. 2018). However, reliability obtained from SORA is still inaccurate due to its approximation on MPP, and MPP-based uncertainty analysis (MPPUA) (Du and Chen 2001), one of uncertainty propagation methods, is often inefficient for accurate statistical information. Several researches suggested improved PATC methods in various ways but without intrinsic modification in uncertainty propagation of linking variables.

Therefore, the proposed research focuses on resolving accuracy issues existing in conventional PATC methods, especially PATC with moment-matching. For this purpose, a concrete framework called sampling-based PATC using multivariate KDE specialized for uncertainty propagation of linking variables is proposed. This allows each subsystem to be optimized more accurately under the scheme of the sampling-based RBDO and makes random linking variables consistent between subsystems. Multivariate kernel density estimation (KDE) for transferring uncertainty of correlated linking variables more accurately to corresponding subsystems and its stochastic sensitivity analysis to perform the sampling-based RBDO are developed in this study. Propagation and coordination for three types of design variables, which are local variables, coupling variables, and shared variables, are strictly categorized depending on how it is manipulated as consistency constraints. Consequently, the sampling-based RBDO and augmented Lagrangian coordination and alternating direction method of multipliers (AL-AD) are successfully combined by exploiting multivariate KDE to connect both methodologies. In other words, individual optimizations of ATC are performed using the sampling-based RBDO to obtain an accurate optimum, and KDE of linking variables connects individual optimizations to satisfy consistency constraints instead of moment-matching.

The article is organized as follows. Brief reviews including existing PATC and sampling-based RBDO are presented in Section 2. In Section 3, the proposed method is presented with key ideas of the new framework. Then, the feasibility and effectiveness of the proposed framework are verified through numerical and engineering examples in Sections 4 and 5. Conclusion and future research are given in Section 6.

2. Overview of Conventional Analytical Target Cascading Methodologies

2.1 Non-hierarchical Analytical Target Cascading (ATC)

The proposed research is originated from the non-hierarchical ATC without a multilevel concept to treat more common structure in the real world (Tosserams et al. 2010). Parent-children subsystems defined under strict conditions with respect to linking variables are unnecessary in the non-hierarchical ATC. Readers can refer to the literature (Kim et al. 2003; Tosserams et al. 2006) for detailed descriptions of hierarchical ATC. Any linked subsystem in the non-hierarchical ATC can communicate with other subsystems directly without any restriction. General structure describing the relationship between neighbors (i.e., linked subsystems) is illustrated in Figure 1. Optimization of a Subsystem *j* in the non-hierarchical ATC can be formulated as (Tosserams et al. 2010)

$$
\begin{aligned}
&\min_{\bar{\mathbf{x}}_j} \; f_j(\bar{\mathbf{x}}_j) + \sum_{n \in R_j} \pi(\mathbf{t}_{nj} - \mathbf{r}_{jn}) + \sum_{m \in T_j} \pi(\mathbf{t}_{jm} - \mathbf{r}_{mj}) \\
&\text{subject to} \;\; \mathbf{g}_j(\bar{\mathbf{x}}_j) \le 0, \;\; \mathbf{h}_j(\bar{\mathbf{x}}_j) = 0 \\
&\text{where} \;\; \pi(\mathbf{c}) = \mathbf{v}^{\mathrm{T}}\mathbf{c} + \left\| \mathbf{w} \circ \mathbf{c} \right\|_2^2 \\
&\qquad \bar{\mathbf{x}}_j = [\mathbf{x}_j, \mathbf{r}_{jn} \,|\, n \in R_j, \mathbf{t}_{jm} \,|\, m \in T_j] \\
&\qquad \mathbf{r}_{jn} = \mathbf{S}_{jn}\mathbf{a}_j(\mathbf{x}_j, \mathbf{t}_{jm} \,|\, m \in T_j) \text{ for } n \in R_j
\end{aligned}
\tag{1}
$$

In Eq. (1), $\bar{\mathbf{x}}_j$ represents the design variables for Subsystem *j*, $\mathbf{x}_j$ represents the local design variables, $\mathbf{r}_{jn}$ represents the responses of Subsystem *j* corresponding to the target $\mathbf{t}_{nj}$ from Subsystem *n*. Similarly, $\mathbf{t}_{jm}$ represents the target corresponding to the response $\mathbf{r}_{mj}$ which is transferred from the Subsystem *m*. The functions f_j, $\mathbf{g}_j$, and $\mathbf{h}_j$ represent the local objective, inequality, and equality constraint functions, respectively. The function $\mathbf{a}_j$ is response function and $\mathbf{S}_{jn}$ is a binary selection matrix that selects components from $\mathbf{a}_j$. The ∘ symbol means a term-by-term multiplication of vectors. The augmented Lagrangian coordination is applied in Eq. (1) where $\mathbf{v}$ is the Lagrange multiplier vector and $\mathbf{w}$ is a penalty weight vector. It should be noted that all design variables in Eq. (1) are deterministic.

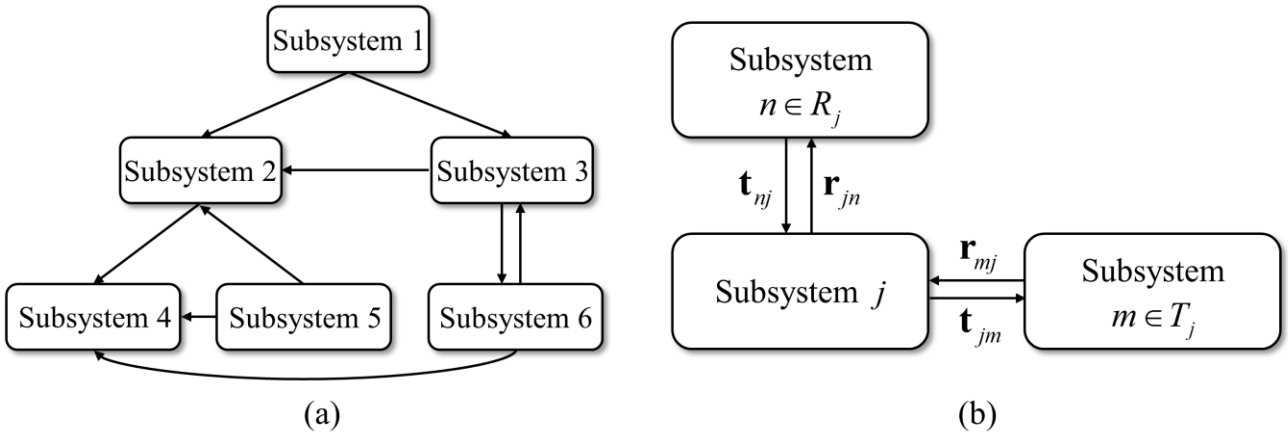

Fig. 1 (a) Functional dependence structure of non-hierarchical ATC and (b) Target and response flow between Subsystem *j* and its neighbors (modified from Tosserams et al. 2010)

2.2 Probabilistic Analytical Target Cascading (PATC) using Moment-matching

PATC using moment-matching combined with AL-AD can be formulated as (Liu et al. 2006; Tosserams et al. 2006)

$$
\begin{aligned}
&\text{given } \boldsymbol{\mu}_{nj}, \boldsymbol{\sigma}^2_{nj}, \boldsymbol{\mu}_{mj}, \boldsymbol{\sigma}^2_{mj} \\
&\min_{\mu_{\bar{\mathbf{X}}_j}} f_j(\mu_{\bar{\mathbf{X}}_j}) + \sum_{n \in R_j} \left(\pi(\boldsymbol{\mu}_{nj} - \boldsymbol{\mu}_{jn}) + \pi(\boldsymbol{\sigma}^2_{nj} - \boldsymbol{\sigma}^2_{jn}) \right) + \sum_{m \in T_j} \left(\pi(\boldsymbol{\mu}_{jm} - \boldsymbol{\mu}_{mj}) + \pi(\boldsymbol{\sigma}^2_{jm} - \boldsymbol{\sigma}^2_{mj}) \right) \\
&\text{subject to } \mu_{\mathbf{g}_j} + k\sigma_{\mathbf{g}_j} \le \mathbf{0} \\
&\text{where } \pi(\mathbf{c}) = \mathbf{v}^{\mathrm{T}}\mathbf{c} + \left\| \mathbf{w} \circ \mathbf{c} \right\|_2^2 \qquad (2) \\
&\bar{\mathbf{X}}_j = [\mathbf{X}_j, \mathbf{R}_{jn} \,|\, n \in R_j, \mathbf{T}_{jm} \,|\, m \in T_j] \\
&\mathbf{R}_{jn} = \mathbf{S}_{jn}\mathbf{a}_j(\mathbf{X}_j, \mathbf{T}_{jm} \,|\, m \in T_j) \text{ for } n \in R_j, \\
&\mathbf{T}_{jm} \sim N(\boldsymbol{\mu}_{jm}, \boldsymbol{\sigma}^2_{jm})
\end{aligned}
$$

In Eq. (2), $\bar{\mathbf{X}}_j$ is the random vector in Subsystem *j*. Among the random design variables, $\mathbf{X}_j$ is the vector of local variables in Subsystem *j* with known parametric distributions. Also, $\mathbf{T}_{jm}$ is assumed to follow a normal distribution with the first two moments from Subsystem *m*, which is denoted as $\boldsymbol{\mu}_{jm}$ and $\boldsymbol{\sigma}^2_{jm}$, respectively. In contrast, $\mathbf{R}_{jn}$ is

the probabilistic response to be computed in Subsystem *j*, and $\boldsymbol{\mu}_{jn}$ and $\boldsymbol{\sigma}_{jn}^2$ are statistical moments used in the consistency constraints. $\mu_{\mathbf{g}_j}$ and $\sigma_{\mathbf{g}_j}$ are mean and standard deviation of the limit-state function in Subsystem *j*, so that probabilistic constraints are estimated by the moment-matching method where *k* is a constant corresponding to the given target reliability level.

The moment-matching method has two accuracy issues. First, the distributions of all matching quantities and constraints need to be close to the normal distribution in order for the method to be accurate. Even if the moment-mating method can be adapted to any parametric distribution, the random responses in the real world may not follow the parametric distribution. Second, the first two statistical moments should have a dominating impact on the optimum (Liu et al. 2006). However, it may not be always satisfied in engineering applications.

2.3 Reliability Analysis and Sampling-based RBDO

Reliability analysis to consider the uncertainties can be categorized into analytical and sampling methods as a whole. The analytical methods have been developed using approximation on limit-state function to estimate the probability of failure (Tu et al. 1999; Adhikari 2004; Lee et al. 2012; Lim et al. 2014; Jung et al. 2019). On the other hands, the sampling methods mainly use random sampling in the probabilistic domain (Denny 2001; Rubinstein and Kroese 2016). Thus, design optimization using the sampling method for reliability analysis is called sampling-based RBDO which is mainly employed in the paper due to its accuracy compared with the analytical methods (Dubourg et al. 2013; Bae et al. 2018; Kang et al. 2019). Reliability analysis and stochastic sensitivity analysis should be iteratively performed in the sampling-based RBDO to deal with probabilistic constraints. Unlike PATC using moment-matching which uses the first two moments of the subsystems, the proposed method applies the sampling-based RBDO to individual optimizations of the subsystems.

In the sampling-based RBDO, the probability of failure can be computed as (Lee et al. 2011)

$$P_F \equiv \Pr[G(\mathbf{X}) > 0] = \int I_{\Omega_F}(\mathbf{x}) f_{\mathbf{X}}(\mathbf{x}) d\mathbf{x} = E\left[I_{\Omega_F}(\mathbf{x}) \right]$$
$$\text{where } I_{\Omega_F}(\mathbf{x}) = \begin{cases} 1, & \mathbf{x} \in \Omega_F \\ 0, & \text{otherwise} \end{cases} \quad (3)$$
$$\Omega_F \equiv \{\mathbf{x} : G(\mathbf{x}) > 0\}$$

In Eq. (3), $\Pr[\bullet]$ and $E[\bullet]$ represent a probability and an expectation measure, respectively; $G(\mathbf{x})$ is the limit-state function; Ω_F is the failure set defined as $G(\mathbf{x}) > 0$; $f_{\mathbf{X}}(\mathbf{x})$ is the joint probability density function (PDF) of $\mathbf{X}$. Moreover, the stochastic sensitivity for the probability of failure is obtained through the first-order score function using PDFs of random design variables (Lee et al. 2011). Since the numerical integration in Eq. (3) would require excessive samplings, surrogate modeling is often employed in the sampling-based RBDO. However, surrogate modeling and sampling strategies are beyond the scope of this research, so that we focused on how to establish an overall framework by connecting PATC and RBDO to alleviate the accuracy issues in the conventional PATC.

3. Sampling-based Probabilistic Analytical Target Cascading with Kernel Density Estimation

3.1 Terminology and Remarks

Each variable and function for the proposed method have to be defined specifically and clearly. Assuming an extensive system with multiple subsystems, three types of variables can be classified in the decomposed subsystems: 1) local variables that belong to a single subsystem only, 2) coupling variables that behave as design variables in a subsystem and as responses in the corresponding subsystem, and 3) shared variables which are design variables in both linked subsystems. Coupling and shared variables are also called linking variables. In order to prevent confusion on defining coupling variables, a coupling variable as a response is denoted as a coupling response hereafter. Detailed notations to describe the proposed formulation are listed in Table 1 (Papalambros and Wilde 2017).

Table 1 Detailed description of notations in the proposed framework

Notation	Description

$\mathbf{X}_j^{Local}$	Random local variable in Subsystem *j*
$\mathbf{X}_{jn}^{Shared} \equiv \mathbf{X}_{nj}^{Shared}$	Random shared variable between Subsystem *j* and Subsystem *n*
$\mathbf{X}_{jn}^{Coup} \equiv \mathbf{Y}_{nj}^{Coup}$	Random coupling variable in Subsystem *j* and coupling response in Subsystem *n*
$\mathbf{Y}_{jn}^{Coup} \equiv \mathbf{X}_{nj}^{Coup}$	Random coupling response in Subsystem *j* and coupling variable in Subsystem *n*
${}^{*}\mathbf{y}_{nj}^{Coup}$	Realizations of coupling response $\mathbf{Y}_{nj}^{Coup}$ received from Subsystem *n*
$\bar{\mathbf{X}}_j = \left[\mathbf{X}_j^{Local}, \mathbf{X}_{jn}^{Coup}, \mathbf{X}_{jn}^{Shared}\right]$	Random design variables in Subsystem *j*
$\hat{p}(\mathbf{x}; \boldsymbol{\mu}_{\mathbf{X}_{jn}^{Coup}}, {}^{*}\mathbf{y}_{nj}^{Coup})$	Multivariate kernel density estimation of $\mathbf{X}_{jn}^{Coup}$ constructed on ${}^{*}\mathbf{y}_{nj}^{Coup}$
$\hat{\mathbf{R}}_{jn}$	Approximated response function to compute coupling response $\mathbf{Y}_{jn}^{Coup}$ in Subsystem *j*
$\hat{\mathbf{G}}_j$	Approximated limit-state function for constraints in Subsystem *j*
$\mathbf{v}$	Lagrange multiplier vector
$\mathbf{w}$	Penalty weight vector
$f_j(\mu_{\bar{\mathbf{X}}_j})$	Local objective function in Subsystem *j*

On the other hand, the coordination algorithm of ATC can be divided into the inner loop and the outer loop to achieve convergence and consistency of the system optimum. In the inner loop, individual optimizations of the subsystem are conducted in the presence of given parameters without any communication. In the outer loop, Lagrange multipliers and penalty weights are updated, and linking variables are transferred. In the perspective of the double-loop scheme, the sampling-based RBDOs are performed in the inner loop of ATC, and uncertainty propagation is performed in the outer loop since uncertainties of linking variables will be propagated after individual RBDOs of all subsystems. Note that the coordination scheme of AL-AD is exploited to the proposed double-loop structure. Therefore, the inner loop for individual optimization and the outer loop for uncertainty quantification and propagation are explained in the subsequent sections

3.2 Basic Formulation for Sampling-based PATC: Inner Loop

In this section, sampling-based RBDO of a general subsystem and how to establish consistency constraints between linking variables are explained. Since the inner loop of PATC indicates the individual RBDO of each

subsystem to obtain the optimum under given Lagrange multiplier, penalty weight, and information on linking variables from the corresponding subsystem. Consequently, the consistency would be gradually decreased through several times of repetitive RBDOs, converging the Lagrange multipliers. Note that there is no communication between subsystems in the inner loop, and thus it is merely sampling-based RBDO in the context of augmented Lagrangian coordination.

3.2.1 Formulation

The proposed optimization formulation of a subsystem with three types of consistency constraints can be expressed as

$$
\begin{aligned}
&\text{given} \quad {}^{*}\mathbf{y}_{nj}^{Coup}, \boldsymbol{\mu}_{\mathbf{X}_{nj}^{Coup}}, \boldsymbol{\mu}_{\mathbf{X}_{nj}^{Shared}} \\
&\text{find} \quad \mu_{\bar{\mathbf{X}}_j} = \left[\boldsymbol{\mu}_{\mathbf{X}_{jn}^{Local}}, \boldsymbol{\mu}_{\mathbf{X}_{jn}^{Coup}}, \boldsymbol{\mu}_{\mathbf{X}_{jn}^{Shared}} \right] \\
&\min_{\mu_{\bar{\mathbf{X}}_j}} \; f_j\left(\mu_{\bar{\mathbf{X}}_j}\right) + \sum_{n \in R_j} \pi\left({}^{*}\bar{\mathbf{y}}_{nj}^{Coup} - \boldsymbol{\mu}_{\mathbf{X}_{jn}^{Coup}} \right) + \pi\left(\boldsymbol{\mu}_{\mathbf{X}_{nj}^{Coup}} - E\left[\mathbf{Y}_{jn}^{Coup} \right] \right) + \pi\left(\boldsymbol{\mu}_{\mathbf{X}_{nj}^{Shared}} - \boldsymbol{\mu}_{\mathbf{X}_{jn}^{Shared}} \right) \\
&\text{subject to} \quad \Pr\left[\hat{\mathbf{G}}_j(\bar{\mathbf{X}}_j) > 0 \right] \le P_F^{\text{Target}} \\
&\text{where} \quad \pi(\mathbf{c}) = \mathbf{v}^{\mathrm{T}}\mathbf{c} + \left\| \mathbf{w} \circ \mathbf{c} \right\|_2^2 \\
&\qquad \bar{\mathbf{X}}_j = \left[\mathbf{X}_j^{Local}, \mathbf{X}_{jn}^{Coup}, \mathbf{X}_{jn}^{Shared} \right], \quad \mathbf{Y}_{jn}^{Coup} = \hat{\mathbf{R}}_{jn}(\bar{\mathbf{X}}_j) \\
&\qquad \mathbf{X}_j^{Local} \sim \zeta_j^{Local}\left(\boldsymbol{\mu}_{\mathbf{X}_j^{Local}}, \boldsymbol{\sigma}^2_{\mathbf{X}_j^{Local}}\right) \\
&\qquad \mathbf{X}_{jn}^{Shared} \sim \zeta_{jn}^{Shared}\left(\boldsymbol{\mu}_{\mathbf{X}_{jn}^{Shared}}, \boldsymbol{\sigma}^2_{\mathbf{X}_{jn}^{Shared}}\right) \\
&\qquad \mathbf{X}_{jn}^{Coup} \sim \hat{p}\left(\mathbf{x}; \boldsymbol{\mu}_{\mathbf{X}_{jn}^{Coup}}, {}^{*}\mathbf{y}_{nj}^{Coup}\right)
\end{aligned}
\tag{4}
$$

In Eq. (4), ζ means any parametric distribution; P_F^{Target} is target probability of failure; $\hat{p}$ is shifted multivariate KDE; $\hat{\mathbf{G}}_j$ and $\hat{\mathbf{R}}_j$ are surrogate models to approximate expensive limit-state function $\mathbf{G}_j$ and coupling response $\mathbf{Y}_{jn}^{Coup}$ in subproblem *j*, respectively. The probabilistic constraints are evaluated through MCS as Eq. (3), and the augmented Lagrangian coordination is used to promote the consistency between linking variables. The purpose of the optimization in Eq. (4) is to find the optimal mean vector of random design variables.

The objective function in Eq. (4) includes a penalty function regarding three types of consistency constraints. Firstly, $\pi\left({}^{*}\bar{\mathbf{y}}_{nj}^{Coup} - \boldsymbol{\mu}_{\mathbf{X}_{jn}^{Coup}} \right)$ is associated with a coupling variable in Subsystem *j* and a coupling response in Subsystem *n*. ${}^{*}\bar{\mathbf{y}}_{nj}^{Coup}$ is the sample mean of ${}^{*}\mathbf{y}_{nj}^{Coup}$ which are the realizations of the random coupling response received from Subsystem *n*, and $\boldsymbol{\mu}_{\mathbf{X}_{jn}^{Coup}}$ is the design vector of coupling variable in Subsystem *j*. The second term $\pi\left(\boldsymbol{\mu}_{\mathbf{X}_{nj}^{Coup}} - E\left[\mathbf{Y}_{jn}^{Coup} \right] \right)$ also corresponds to a coupling variable in the opposite way. The expectation of coupling response $\mathbf{Y}_{jn}^{Coup}$ should be consistent with $\boldsymbol{\mu}_{\mathbf{X}_{nj}^{Coup}}$ that is given from Subsystem *n*. Thus, it is a coupling variable in Subsystem *n* and a coupling response in Subsystem *j*. The third term $\pi\left(\boldsymbol{\mu}_{\mathbf{X}_{nj}^{Shared}} - \boldsymbol{\mu}_{\mathbf{X}_{jn}^{Shared}} \right)$ is related to a shared variable. Since the distribution of the shared variable is known, uncertainty propagation using KDE can be performed accurately by statistical moments, so that only mean vector is used in the consistency constraint.

Note that the distribution of coupling variables is denoted as $\hat{p}(\mathbf{x}; \boldsymbol{\mu}_{\mathbf{X}_{jn}^{Coup}}, {}^{*}\mathbf{y}_{nj}^{Coup})$ defined as shifted multivariate KDE of coupling variable $\mathbf{X}_{jn}^{Coup}$ constructed from ${}^{*}\mathbf{y}_{nj}^{Coup}$. This procedure indicates that statistical information of coupling variable in Subsystem *j* is received from Subsystem *n*, but its design vector (i.e., mean vector of KDE) can change because it is one of design variables to be optimized. On the other hand, the distribution of the coupling response also has to move toward the given mean vector of coupling variable from the corresponding system. The uncertainty propagation and communication of coupling variables and responses will be described in Section 3.3.

3.2.2 Subsystem Composition

Detailed composition of a general subsystem is illustrated in a single subsystem in Figure 2 where subscripts for subsystem index are omitted. A vector of local variables is denoted as $\mathbf{X}^{Local}$ which contains all random local variables. A vector of shared variables is denoted as $\mathbf{X}^{Shared}$ imposed to be consistent with linked

subsystems. A vector of coupling variables is denoted as $\mathbf{X}^{Coup}$. Since it is not a design variable in the system-level, the variability of $\mathbf{X}^{Coup}$ should be assigned by the corresponding subsystem as a coupling response through multivariate KDE. On the other hands, responses to be computed in the subsystem can be categorized into limit-state function and coupling responses. The limit-state function $\mathbf{G}^{Perf}$ is involved in probabilistic constraints for the optimization, and the coupling response $\mathbf{Y}^{Coup}$ is computed to propagate uncertainty. In other words, the limit-state function is used only within each RBDO of a subsystem as a constraint, so that it is not involved in a linking variable.

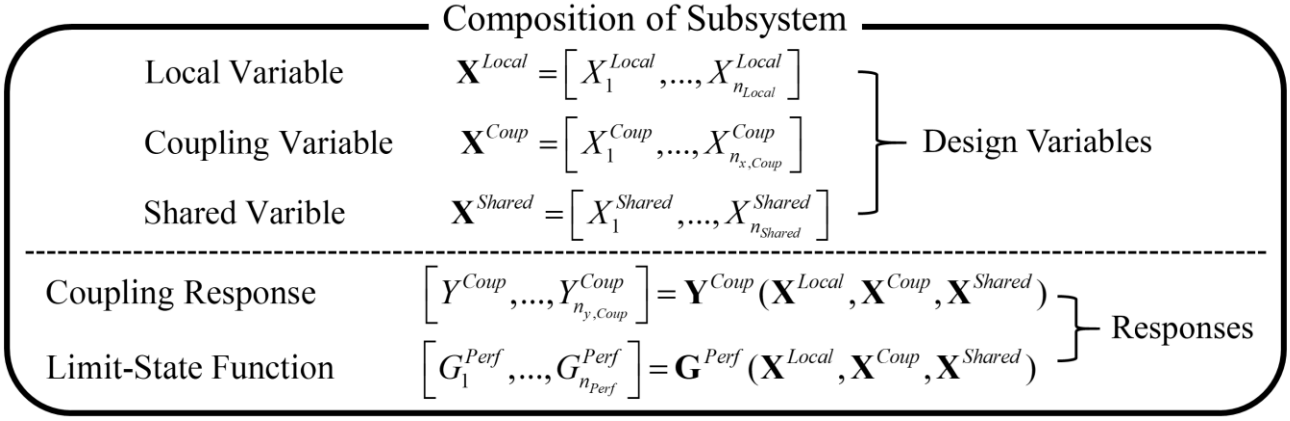

Fig. 2 Composition of a general subsystem

Figure 3 shows a simple scheme of three subsystems. Each subsystem has own local variable, and there are two coupling variables and one shared variable. The arrow between two subsystems indicates the consistency constraint. Subsystems 1 and 2 are linked with a coupling variable. The correlated coupling responses in Subsystem 2 and 3 are propagated to Subsystem 1 as the 2-dimensional histogram in Figure 3, and Subsystem 1 is optimized with the propagated variability of Y_{21}^{Coup} and Y_{31}^{Coup} returning $\mu_{X_{12}^{Coup}}$ and $\mu_{X_{13}^{Coup}}$ to Subsystems 2 and 3. Therefore, the consistency constraint in Subsystem 2 and 3 can be expressed as $\mu_{X_{12}^{Coup}} - E\left[Y_{21}^{Coup}\right]$ and $\mu_{X_{13}^{Coup}} - E\left[Y_{31}^{Coup}\right]$, respectively. Note that the coupling responses are assumed to be correlated since there are shared variable in

Subsystem 2 and 3, which is the reason why the multivariate KDE should be used. On the other hand, Subsystems 2 and 3 are linked with a shared variable whose distribution is already known. Hence, only mean is transferred, so that the consistency constraint is denoted as $\mu_{X_{23}^{Shared}} - \mu_{X_{32}^{Shared}}$.

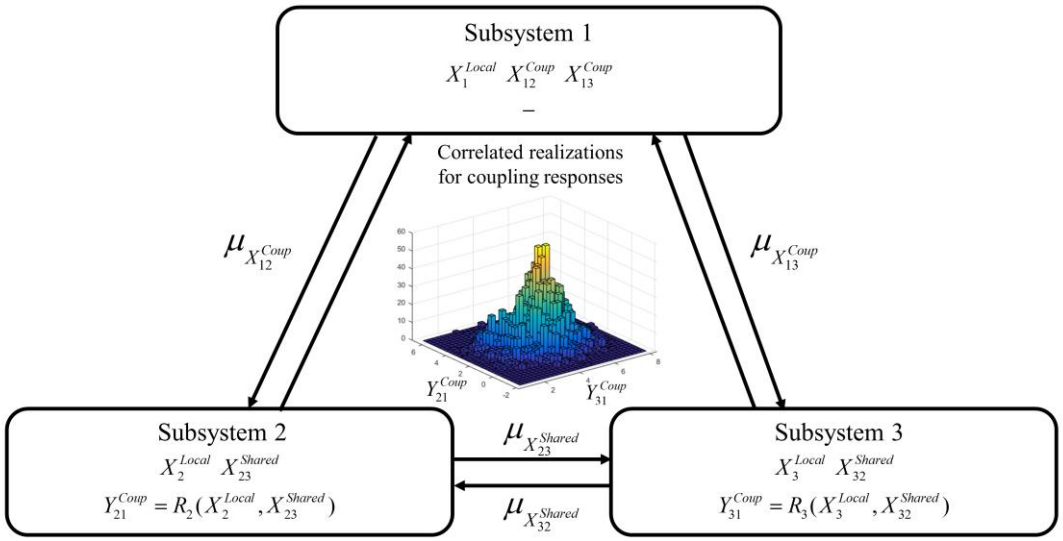

Fig. 3 Flow of linking variables between linked subsystems

3.2.3 Surrogate Modeling

Surrogate modeling is utilized in the proposed PATC framework especially in the inner loop to alleviate the expensive computational cost. For further efficiency improvement, sequential sampling strategies are often combined with surrogate modeling. There have been extensive researches on effective sequential sampling in which the new sample location is explored to greatly increase the accuracy of surrogate model, but the constraint boundary sampling (CBS) with local window is adapted in this study to enhance accuracy and efficiency of surrogate models. The CBS criterion is formulated as (Lee and Jung 2008; Chen et al. 2014)

$$CBS = \begin{cases} \sum_{i=1}^{N} \phi\left(\dfrac{\hat{G}_i(\mathbf{x})}{\sqrt{\sigma^2_{\hat{G}_i}}}\right) \cdot D & \text{if } \hat{G}_i(\mathbf{x}) \geq 0,\ \forall i \\ 0 & \text{otherwise} \end{cases} \tag{5}$$

where D is the minimal distance from the current sample point to the existing sample points and $\hat{G}_i(\mathbf{x})$ is the prediction of the limit-state function at the current point $\mathbf{x}$ and $\sigma^2_{\hat{G}_i}$ indicates the estimated variance of the current sample point. In the remainder of paper, the second order polynomial basis function and Gaussian correlation function are used in Kriging model for the mean structure and correlation function, respectively.

One important thing to be discussed when using surrogate models is that the design space can be partitioned in the ATC structure. This means that high-dimensional design space can be decomposed into several low-dimensional design spaces, and unlike existing ATC, it may be efficient than even All-in-One (AiO) which optimizes the entire system at once in the high-dimensional design space since the number of samplings to achieve acceptable level of accuracy increases exponentially with dimensions, called “the curse of dimensionality”. Efficiency comparison with AiO is beyond the scope of the paper, so we will use it for reference only.

3.3 Uncertainty Propagation and Sensitivity Analysis for Kernel Density Estimation: Outer Loop

In the outer loop of the proposed PATC, mean vectors including local, shared, and coupling variables and nonparametric distributions of coupling responses have to be exchanged, and the corresponding Lagrange multipliers and penalty weights are appropriately updated using AL-AD. Even though the sampling-based RBDO can be adapted into the individual optimizations of subsystems, ATC structure always has linking variables transferred from linked subsystems. Therefore, the uncertainty propagation of the linking variable, the key concept of the proposed framework, have to be developed preferentially. However, a coupling variable is not a design variable in the system-level but an intermediate response due to decomposition which is a function of design variables. Thus, explicit expression of its uncertainty necessary for stochastic sensitivity analysis of RBDO cannot be achieved. In the proposed method, uncertainty quantification and propagation of a coupling variable are

conducted using KDE.

Kernel density estimation (KDE) is a nonparametric method to estimate underlying PDF of a random variable based on given samples drawn from the true but unknown distribution (Chen 2017; Silverman 2018) as the summation of kernel functions generated by each sample. Thus, it facilitates to estimate the distribution of coupling variable based on the realizations from the corresponding subsystem. In addition, there are several coupling variables transferred from a single subsystem or sharing the source of uncertainty for shared variables. It means that multiple coupling variables could be correlated to each other in a single subsystem. Thus, we exploit both univariate and multivariate KDE for uncertainty propagation of coupling variables according to the presence of correlation. Since the multivariate KDE is much complicated and time-consuming, it is recommended to select the method according to the configuration of the decomposed system. The correlation of coupling variables in moment-matching has been treated in the literature (Xiong et al. 2010).

3.3.1 Shifted Kernel Density Estimation

The univariate KDE using Gaussian kernel function for a single independent coupling variable when there is no correlation between coupling variables can be formulated as

$$\begin{aligned}\hat{p}(x;{}^{*}\mathbf{y}^{Coup}) &= \frac{1}{n}\sum_{i=1}^{n} K_h\left(x - {}^{*}y^{Coup,(i)}\right) \\ &= \frac{1}{\sqrt{2\pi}nh}\sum_{i=1}^{n}\exp\left(-\frac{1}{2h^2}\left(x - {}^{*}y^{Coup,(i)}\right)^2\right)\end{aligned} \tag{6}$$

where n is the number of given samples, ${}^{*}\mathbf{y}^{Coup} = \left[{}^{*}y^{Coup,(1)},...,{}^{*}y^{Coup,(n)}\right]^{\mathrm{T}}$ represents the vector of given samples for a single coupling variable. ${}^{*}y^{Coup,(i)}$ is i-th sample, and h is the positive smoothing parameter (i.e., bandwidth). It can be seen from Eq. (6) that the kernel function only depends on the smoothing parameter with the given samples. The smoothing parameter will be computed using the Rule-of-Thumb since the true distribution of a linking variable is unknown given by (Silverman 2018)

$$h = \left(\frac{4\hat{\sigma}^5}{3n} \right)^{\frac{1}{5}} \approx 1.06\hat{\sigma} n^{-\frac{1}{5}} \tag{7}$$

where $\hat{\sigma}^2$ is the sample variance and n is the number of samples. The Rule-of-Thumb assumed that the true distribution is close to the normal distribution, but it gives a plausible PDF for any true distribution. The detailed description of KDE and methods to determine an optimal smoothing parameter to reduce mean integrated square error (MISE) can be seen in the literature (Chen 2017; Silverman 2018).

The multivariate KDE for multiple correlated coupling variables with a set of given samples can be written as

$$\begin{aligned} \hat{p}(\mathbf{x}; {}^{*}\mathbf{y}^{Coup}) &= \frac{1}{n}\sum_{i=1}^{n} K_H \left(\mathbf{x} - {}^{*}\mathbf{y}^{Coup,(i)} \right) \\ &= \frac{1}{n}(2\pi)^{-m/2} |H|^{-1/2} \sum_{i=1}^{n} \exp\left(-\frac{1}{2} (\mathbf{x} - {}^{*}\mathbf{y}^{Coup,(i)})^{\mathrm{T}} H^{-1} (\mathbf{x} - {}^{*}\mathbf{y}^{Coup,(i)}) \right) \end{aligned} \tag{8}$$

where n is the number of samples; m is the number of correlated coupling variables; H is the bandwidth matrix to be calculated; ${}^{*}\mathbf{y}^{Coup,(i)} = \left[{}^{*}y_1^{Coup,(i)}, ..., {}^{*}y_m^{Coup,(i)} \right]^{\mathrm{T}}$ represents the i-th sample of m correlated coupling variable; ${}^{*}\mathbf{y}^{Coup} = \left[{}^{*}\mathbf{y}^{Coup,(1)}, ..., {}^{*}\mathbf{y}^{Coup,(n)} \right]^{\mathrm{T}}$ is a matrix composed of n number of samples. In other words, n number of m-dimensional sample data for coupling variables are used to establish the multivariate KDE.

If the coupling variable has to estimate PDF from a linked subsystem as Eqs. (6) or (8), it should be shifted based on the current design point since coupling variables are also design variable to be optimized. It means that the statistical characteristics of the coupling responses should be maintained except for the design vector (i.e., mean vector). In consequence, the joint PDF of correlated coupling variables in case of multivarite KDE and current design vector can be expressed as

$$\begin{gathered} \hat{p}(\mathbf{x}; \boldsymbol{\mu}_{\mathbf{X}^{Coup}}, {}^{*}\mathbf{y}^{Coup}) = \frac{1}{n}(2\pi)^{-m/2} |H|^{-1/2} \sum_{i=1}^{n} \exp\left(-\frac{1}{2} (\mathbf{x} - \mathbf{s}^{(i)})^{\mathrm{T}} H^{-1} (\mathbf{x} - \mathbf{s}^{(i)}) \right) \\ \text{where } \mathbf{s}^{(i)} = {}^{*}\mathbf{y}^{Coup,(i)} - {}^{*}\overline{\mathbf{y}}^{Coup} + \boldsymbol{\mu}_{\mathbf{X}^{Coup}} \end{gathered} \tag{9}$$

The *i*-th shifted samples denoted as $\mathbf{s}^{(i)}$ is defined to reflect the current mean vector of coupling variables denoted as $\boldsymbol{\mu}_{\mathbf{X}^{Coup}}$ to samples given from corresponding subsystems, and ${}^{*}\overline{\mathbf{y}}^{Coup} = \left[{}^{*}\overline{\mathbf{y}}_1^{Coup}, \ldots {}^{*}\overline{\mathbf{y}}_m^{Coup} \right]^{\mathrm{T}}$ is the sample mean vector of *m* correlated design variables. It indicates that given samples are equally shifted according to current design vector of coupling variables. Through the shifting of the samples, only the numerical expectation of KDE is changed (Silverman 2018). In the proposed method, the consistency constraint can be arranged with the mean, but uncertainties are transferred as a nonparametric distribution without loss of any statistical information unlike PATC using moment-matching.

3.3.2 Sensitivity Analysis for Kernel Density Estimation

To perform sampling-based RBDO in the proposed PATC, stochastic sensitivity for probabilistic constraints with respect to design vector needs to be estimated accurately. When distributions of random design variables are known, stochastic sensitivities using the first-order score function with respect to the mean vector can be obtained even if input random variables are correlated (Lee et al. 2011; Cho et al. 2016). However, since the coupling variable follows the KDE in the proposed PATC, analytical sensitivity analysis for KDE is derived in this section, and its accuracy is verified in comparison with the finite difference method (FDM) in Section 4.

Stochastic sensitivity analysis of the probability of failure with respect to the mean of the *j*-th random variable including local and shared variables whose distributions are known is obtained as

$$\begin{aligned} \frac{\partial P_F}{\partial \mu_j} &= \frac{\partial}{\partial \mu_j} \int I_{\Omega_F}(\mathbf{x}) f_{\mathbf{X}}(\mathbf{x};\boldsymbol{\mu}) \mathrm{d}\mathbf{x} \\ &= \int I_{\Omega_F}(\mathbf{x}) \frac{\partial \ln f_{\mathbf{X}}(\mathbf{x};\boldsymbol{\mu})}{\partial \mu_j} f_{\mathbf{X}}(\mathbf{x};\boldsymbol{\mu}) \mathrm{d}\mathbf{x} \\ &= E\left[I_{\Omega_F}(\mathbf{x}) \frac{\partial \ln f_{\mathbf{X}}(\mathbf{x};\boldsymbol{\mu})}{\partial \mu_j} \right] \end{aligned} \tag{10}$$

The partial derivative of the log function of joint PDF with respect to mean of *j*-th random variable is called first-order score function. It has been well derived in the literature when input distribution is known parametric

distribution, so that the stochastic sensitivity analysis with respect to local and shared variables can be performed (Lee et al. 2011).

However, the distribution of coupling variables is estimated by KDE. In the case of independent coupling responses, the first-order score function of univariate KDE with respect to *j*-th mean vector can be derived as

$$\begin{aligned}\frac{\partial \ln f_{\mathbf{X}}(\mathbf{x};\boldsymbol{\mu})}{\partial \mu_j} &\equiv \frac{\partial \ln \hat{p}(x;{}^{*}\mathbf{y}^{Coup})}{\partial \mu_j} \\ &= \sum_{i=1}^{n} \frac{\partial \ln \hat{p}}{\partial {}^{*}y^{Coup,(i)}} \frac{\partial {}^{*}y^{Coup,(i)}}{\partial \mu_j} \\ &= \sum_{i=1}^{n} \frac{x - {}^{*}y^{Coup,(i)}}{\sqrt{2\pi} n h^3 \hat{p}} \exp\left(-\frac{1}{2h^2}(x - {}^{*}y^{Coup,(i)})^2 \right)\end{aligned} \tag{11}$$

since the KDE is a function of samples where ${}^{*}\mathbf{y}^{Coup}$ represents *n* samples of a coupling response, and *h* is the smoothing parameter. It is noted that change of mean vector for KDE represents all data are shifted simultaneously, so that the partial derivative with respect to the *j*-th mean vector, $\frac{\partial {}^{*}y^{Coup,(i)}}{\partial \mu_j}$ is equal to one. Plugging the first-order score function of KDE with respect to independent random variables in Eq. (11) into Eq. (10) yields sensitivity of the probability of failure for independent coupling variables.

In the same context, it can be extended to development for first-order score function of multivariate KDE to handle the correlated coupling variables. Note that the correlation would exist when there is a shared source of uncertainty, and thus the designer should confirm it before the optimizaiton. From Eq. (8), it can be written as

$$\begin{aligned}\frac{\partial \ln f_{\mathbf{X}}(\mathbf{x};\boldsymbol{\mu})}{\partial \mu_j} &\equiv \frac{\partial \ln \hat{p}(\mathbf{x};{}^{*}\mathbf{y}^{Coup})}{\partial \mu_j} \\ &= \sum_{i=1}^{n} \frac{1}{\hat{p}} \frac{\partial \hat{p}}{\partial {}^{*}y_j^{Coup,(i)}} \frac{\partial {}^{*}y_j^{Coup,(i)}}{\partial \mu_j} \\ &= \sum_{i=1}^{n} \frac{1}{\sum_{k=1}^{n} a^{(k)}} \frac{\partial a^{(i)}}{\partial {}^{*}y_j^{Coup,(i)}}\end{aligned} \tag{12}$$

where ${}^{*}y_j^{Coup,(i)}$ is *i*-th sample of *j*-th coupling variable. Since multivariate KDE is a function of $a^{(i)}$ where

$$a^{(i)} = \exp\left(-\frac{1}{2}(\mathbf{x} - {}^{*}\mathbf{y}^{Coup,(i)})^{\mathrm{T}} H^{-1} (\mathbf{x} - {}^{*}\mathbf{y}^{Coup,(i)}) \right) \tag{13}$$

defined as a function of *i*-th sample ${}^{*}\mathbf{y}^{Coup,(i)}$ and **x**. As shown in Eq. (12), the partial derivative of each sample with respect to mean is equal to one, and the only partial derivative of $a^{(i)}$ is derived as

$$\begin{aligned} \frac{\partial a^{(i)}}{\partial {}^{*}y_j^{Coup,(i)}} &= \frac{\partial}{\partial {}^{*}y_j^{Coup,(i)}} \left(\exp\left(-\frac{1}{2}(\mathbf{x} - {}^{*}\mathbf{y}^{Coup,(i)})^{\mathrm{T}} H^{-1} (\mathbf{x} - {}^{*}\mathbf{y}^{Coup,(i)}) \right) \right) \\ &= -\frac{a^{(i)}}{2} \frac{\partial (\mathbf{x} - {}^{*}\mathbf{y}^{Coup,(i)})^{\mathrm{T}} H^{-1} (\mathbf{x} - {}^{*}\mathbf{y}^{Coup,(i)})}{\partial {}^{*}y_j^{Coup,(i)}} \\ &= a^{(i)} \left(\mathbf{x} - {}^{*}\mathbf{y}^{Coup,(i)} \right)^{\mathrm{T}} H_j^{-1} \end{aligned} \tag{14}$$

where H_j^{-1} is *j*-th column vector of H^{-1}. Using Eq. (14), the first-order score function of multivariate KDE for coupling variable finally can be arranged as

$$\begin{aligned} \frac{\partial \ln \hat{p}(\mathbf{x}; {}^{*}\mathbf{y}^{Coup})}{\partial \mu_j} &= \sum_{i=1}^{n} \frac{a^{(i)}}{\sum_{k=1}^{n} a^{(k)}} \left(\mathbf{x} - {}^{*}\mathbf{y}^{Coup,(i)} \right)^{\mathrm{T}} H_j^{-1} \\ &= \frac{1}{\sum_{k=1}^{n} a^{(k)}} \left[a^{(1)}, a^{(2)}, ..., a^{(n)} \right] \begin{pmatrix} x_1 - {}^{*}y_1^{(1)} & \cdots & x_1 - {}^{*}y_1^{(n)} \\ \vdots & \ddots & \vdots \\ x_m - {}^{*}y_m^{(1)} & \cdots & x_m - {}^{*}y_m^{(n)} \end{pmatrix}^{\mathrm{T}} H_j^{-1} \end{aligned} \tag{15}$$

Consequently, the coupling variables can be employed to sampling-based RBDO with analytical sensitivity analysis using first-order score function for univariate KDE in Eq. (11) and multivariate KDE in Eq. (15).

This procedure for sensitivity analysis is the reason why the statistical representation of samples is necessary. Since KDE of coupling variables is established on the realizations of coupling responses from the corresponding subsystem, it can be directly used for computing probability of failure. However, its stochastic sensitivity analysis which requires the first-order score function cannot be explicitly defined without density estimation. To conclude, KDE is employed for providing accurate sensitivity of reliability rather than estimating reliability itself.

3.4 Flowchart of Methodology

This section explains the proposed algorithm in detail using a flowchart. Figure 4 describes the overall flowchart of the proposed PATC. First, deterministic optimizations of individual subsystems while improving Kriging models have to be performed iteratively, and thus the Lagrange multipliers and the penalty weights are updated using AL-AD. Once the deterministic ATC successfully converges to the optimum, it becomes the initial point of the sampling-based PATC. It is noted that FEA is performed only on the specific sampling points for improving the Kriging models, and the sampling-based RBDO is performed using the Kriging models of coupling responses and limit-state function for probabilistic constraints. Especially, the realizations of coupling responses are propagated to corresponding subsystems, and thus the KDE for coupling variable is established to perform reliability analysis and sensitivity analysis will be carried out iteratively. The scheme of updating Lagrange multiplier and penalty weight is still maintained in PATC. Notably, the determination of the surrogate model and the sequential sampling strategy is also critical from the perspective of accuracy and convergence, but it is additional implementation for the proposed method. Thus, any other types of improved sampling method and surrogate modeling can be used in the proposed framework. The main contribution of the proposed method is to suggest the KDE for quantifying the uncertainty of coupling variable in individual RBDOs of subsystems.

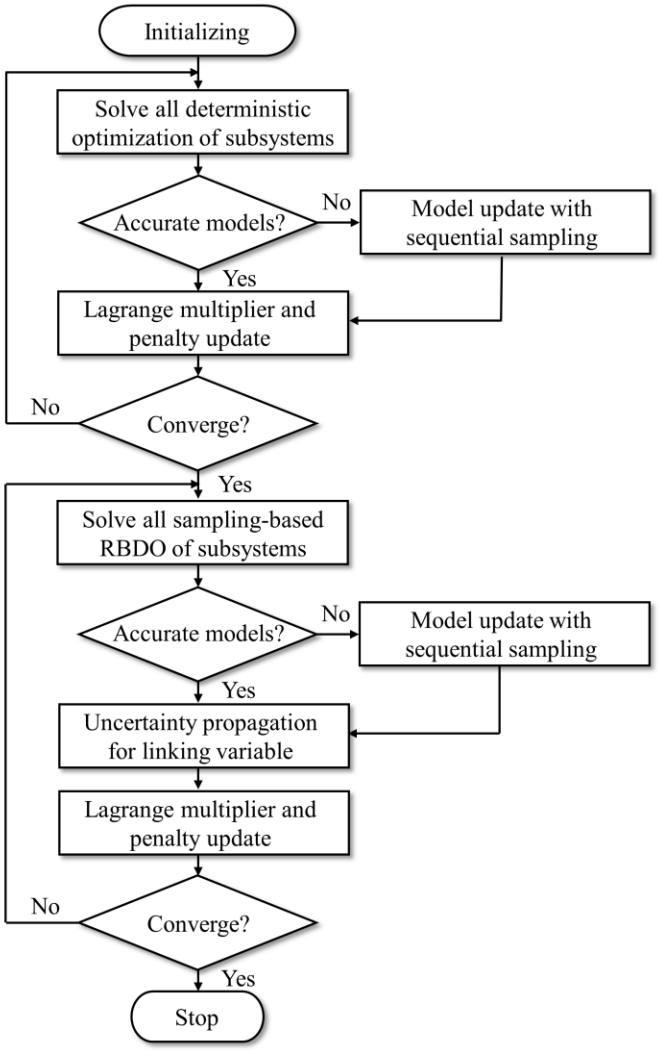

Fig. 4 Overall flowchart of the proposed PATC

4. Numerical Examples

In this section, two mathematical examples are made to verify the proposed method including the sensitivity analysis and the entire optimization compared with existing methods. The first example is related to the univariate KDE since it has a single coupling response, and the second example is involved in multivariate KDE where the coupling responses from two subsystems are correlated due to the shared variable. It can be seen that the proposed method can give accurate results employing KDE to quantify the uncertainty of coupling variables.

4.1 3-dimensional Mathematical Example

A 3-dimensional mathematical example is employed to demonstrate the feasibility of the developed framework compared with All-in-One (AiO) which means the system level optimization combining all subsystems and PATC using moment-matching. In addition, the proposed sensitivity analysis for univariate KDE is verified. It is shown that the proposed framework is capable of providing high accuracy through the uncertainty propagation of nonparametric distributions without any loss of information unlike the moment-matching method.

4.1.1 Formulation of Decomposed 3-dimensional Mathematical Example

The decomposed structure of 3-dimensional RBDO has three types of design variables and two types of responses. There is no shared variable, and Subsystem 1 has a coupling response, and Subsystem 2 has the corresponding coupling variable. There is one consistency constraint with respect to the coupling variable vanished in the system-level optimization.

The optimization of Subsystem 1 is formulated as

$$
\begin{aligned}
\underset{\mu_{X_1},\mu_{X_2}}{\text{minimize}} \quad & -\frac{(\mu_{X_1}+\mu_{X_2}-10)^2}{30}-\frac{(\mu_{X_1}-\mu_{X_2}+10)^2}{120} \\
\text{subject to} \quad & \Pr[G_i(\mathbf{X})>0]\le 0.05 \quad \text{for } i=1,2,3 \\
\text{where} \quad & G_1(\mathbf{X}) = 1-\frac{X_1^2 X_2}{20} \\
& G_2(\mathbf{X}) = -1+(0.9063X_1+0.4226X_2-6)^2+(0.9063X_1+0.4226X_2-6)^3- \\
& \qquad 0.6(0.9063X_1+0.4226X_2-6)^3-(-0.4226X_1+0.9063X_2) \\
& G_3(\mathbf{X}) = 1-\frac{80}{X_1^2+8X_2+5} \\
& Y_1(X_1,X_2) = \frac{2X_1^2-X_2}{10} \\
& X_1 \sim N(\mu_{X_1},0.5^2),\ X_2 \sim N(\mu_{X_2},0.5^2)
\end{aligned}
\tag{16}
$$

In Eq. (16), $Y_1(X_1, X_2)$ is the coupling response to be transferred to Subsystem 2. Only local variables are random design variables in Subsystem 1. The target probability of failure is set to 5.00 % for three constraints.

Similarly, the optimization of Subsystem 2 is formulated as

$$
\begin{aligned}
\underset{\boldsymbol{\mu}_{\mathbf{X}}}{\text{minimize}} \quad & \mu_{X_3} + \mu_{X_1^{Coup}} \\
\text{subject to} \quad & \Pr[G_i(\mathbf{X}) > 0] \le 0.05 \quad \text{for } i = 4,5 \\
\text{where} \quad & G_4(\mathbf{X}) = 1 - \frac{X_3^2 X_1^{Coup}}{20} \\
& G_5(\mathbf{X}) = 1 - \frac{(X_3 + X_1^{Coup} - 10)^2}{30} - \frac{(X_3 - X_1^{Coup} + 10)^2}{120} \\
& X_3 \sim N(\mu_{X_3}, 0.5^2) \\
& X_1^{Coup} \sim \hat{p}(x; \mu_{X_1^{Coup}}, {}^{*}\mathbf{y}_1)
\end{aligned}
\tag{17}
$$

In Eq. (17), X_1^{Coup} is the coupling variable and its uncertainty is described with the shifted KDE explained in Section 3.3.1. ${}^{*}\mathbf{y}_1$ is given realizations of a coupling response from Subsystem 1. There are two random design variables which are a local variable and coupling variable with no coupling response, and other properties are analogous with Subsystem 1. It is noted that Subsystems 1 and 2 can be combined with the substitution of the coupling response $Y_1(X_1, X_2)$ as a function of design variables, and thus it would become 3-dimensional RBDO problem.

4.1.2 Validation of Sensitivity Analysis for Univariate Kernel Density Estimation

In this section, the accuracy of the proposed sensitivity analysis is compared with numerical sensitivity analysis using G_1 and G_2 in Eq. (16). Variability of X_1 is quantified by KDE with 50 samples drawn from the known parametric distribution, and X_2 is assumed to follow a normal distribution. Comparison tests are performed by varying the true distribution of X_1 such as normal, lognormal, and Gumbel distributions, and the results are compared with FDM using various perturbations such as 1.0%, 0.5%, and 0.1%. The number of samples drawn from KDE and the normal distribution to compute the probability of failure is 10^7 at two arbitrary design points which are $\mathbf{d}_1 = [4.56, 1.86]^{\mathrm{T}}$ and $\mathbf{d}_2 = [4.32, 1.95]^{\mathrm{T}}$ where the standard deviation is 0.5 for both random variables.

Table 2 shows the results of the proposed and numerical sensitivity analysis for G_1 and G_2 in Eq. (16). Discrepancies between two sensitivity analysis results in the case of 0.1% perturbation are also shown in

parenthesis. Obviously, low discrepancy can confirmed the correct derivation of proposed sensitivity analysis. The numerical sensitivity analysis is performed using the fixed random seed to eliminate sampling uncertainty, and the proposed method shows accurate results regardless of the true distribution type or design point location.

Table 2 Results of sensitivity analysis with respect to univariate KDE

True Distribution	Design Sensitivity	G_1 at $\mathbf{d}_1$	G_2 at $\mathbf{d}_1$	G_1 at $\mathbf{d}_2$	G_2 at $\mathbf{d}_2$
Normal	FDM (1.0%)	-0.0975	0.0823	-0.1287	0.0275
	FDM (0.5%)	-0.1006	0.0798	-0.1314	0.0264
	FDM (0.1%)	-0.1027	0.0774	-0.1346	0.0249
	Proposed	-0.1020 (0.68%)	0.0764 (1.30%)	-0.1351 (0.37%)	0.0250 (0.40%)
Lognormal	FDM (1.0%)	-0.0987	0.0768	-0.1305	0.0291
	FDM (0.5%)	-0.1012	0.0742	-0.1340	0.0278
	FDM (0.1%)	-0.1037	0.0724	-0.1395	0.0272
	Proposed	-0.1026 (1.07%)	0.0721 (0.41%)	-0.1365 (2.19%)	0.0270 (0.74%)
Gumbel	FDM (1.0%)	-0.0951	0.0784	-0.1338	0.0339
	FDM (0.5%)	-0.0975	0.0761	-0.1370	0.0333
	FDM (0.1%)	-0.1012	0.0752	-0.1381	0.0330
	Proposed	-0.1001 (1.09%)	0.0727 (3.43%)	-0.1401 (1.42%)	0.0322 (2.58%)

4.1.3 Results of Sampling-based PATC

The optimum of AiO representing system-level optimization is $[3.7549,\ 2.6423,\ 4.0267]^{\mathrm{T}}$ which can be thought as true optimum. It is obtained from a single 3-dimensional optimization using true mathematical functions since it is the reference results to validate the accuracy of ATC optimum rather than efficiency. As mentioned before, the proposed method uses the optimum of deterministic ATC as the initial design. In each 2-dimensional subsystem, grid sampling with 5-level full factorial design is used to generate initial samples, which means that 25 samples are used to construct initial Kriging models for the constraints and coupling response as shown in Figure 5. The solid and dotted lines in the figure mean the true and approximated limit-state functions by the Kriging model using 25 samples marked as black solid circles, respectively. The accuracy of the limit-state function seems low, but it could be improved through sequential sampling.

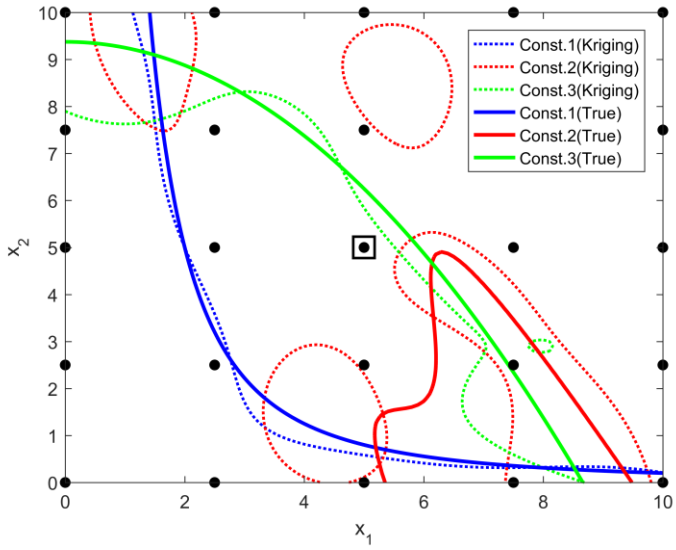

Fig. 5 True and approximated limit-state functions in Subsystem 1

Using the approximated limit-state functions in Figure 5, the proposed PATC is performed based on the algorithm in Figure 4. The tolerance for convergence is set to 5×10^{-3}, the number of MCS samples is 5×10^{5}, and the number of samples for the stochastic sensitivity proposed in Section 3.3.2 is 10^{4}. All initial Lagrange multipliers and penalty weights are set to 1 and 0, respectively. A fixed local window whose radius is $0.3\beta_t$ for deterministic ATC and $1.6\beta_t$ for PATC is used. Note that local window is only used to restrict the range of sequential sampling.

Figure 6 illustrates additional samples, updated Kriging model as dotted lines, and the design point in Subsystem 1 at the end of each process of ATC and sampling-based PATC. It is shown from the figure that the additional samples are located in the vicinity of the limit-state, and the accuracy is partially improved. Table 4 shows optimization results of the proposed method. From Tables 3, it can be seen that the optimum from the proposed PATC is very close to the ones by AiO. From Table 4 which shows optimization results by PATC using moment-matching, the probability of failure at the optimum is inaccurate due to the normality assumption on the coupling variable. It is noted that only mean is used to construct the consistency constraint since the standard

deviation goes to zero during PATC using moment-matching. Therefore, the standard deviation is merely given from Subsystem 1. Figure 7 shows the difference between two methods in the density estimation of the coupling variable. It is because PATC using moment-matching assumes the distribution as a normal distribution with estimated mean and variance, whereas the proposed PATC estimates the distribution using KDE showing the good agreement at the optimum.

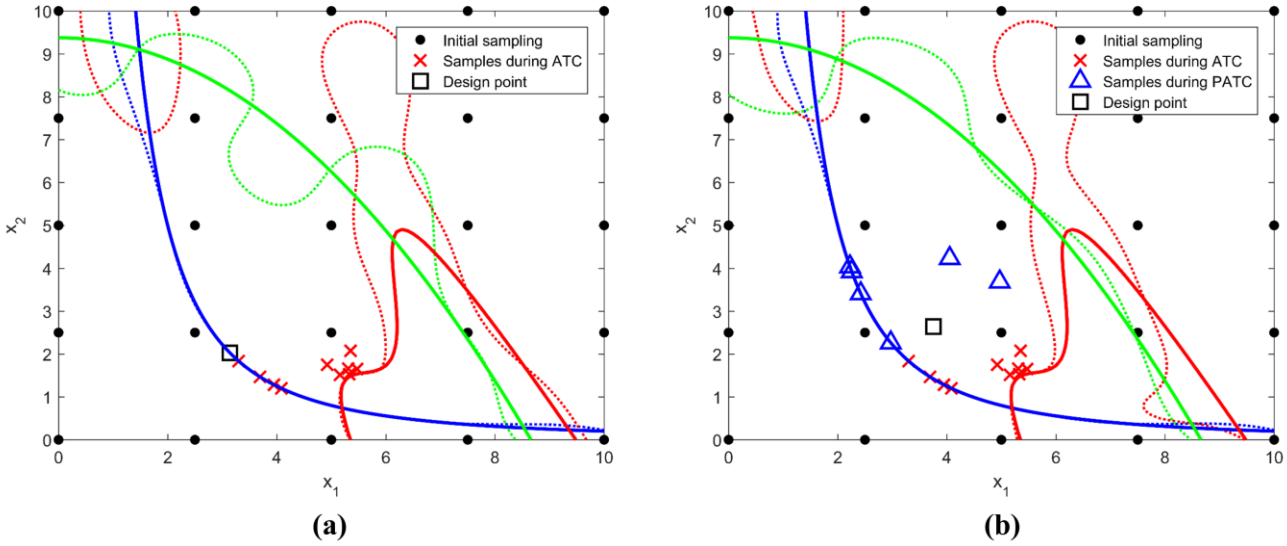

Fig. 6 Optimum and additional samples in the design space of Subsystem 1: (a) ATC (b) Sampling-based PATC

Table 3 Optimization results of the proposed sampling-based PATC

	Subsystem 1	Subsystem 2
Initial grid samples	25 (5^2)	25 (5^2)
Additional samples during ATC	10	2
Additional samples during PATC	6	6
Total samples	41	33
Mean of coupling variable	2.6056	2.6033
Optimum	$[3.7550, 2.6438, 4.0323]^T$	
Probability of failure (%)	[5.02, 4.95, 5.01]	

Table 4 Optimization results of PATC using moment-matching

	Results
Moments of coupling variable	$\mu = 2.6676, \sigma^2 = 0.7647$

Optimum	$[3.7970, 2.5855, 4.0660]^T$
Probability of failure (%)	[5.06, 3.89, 5.94]

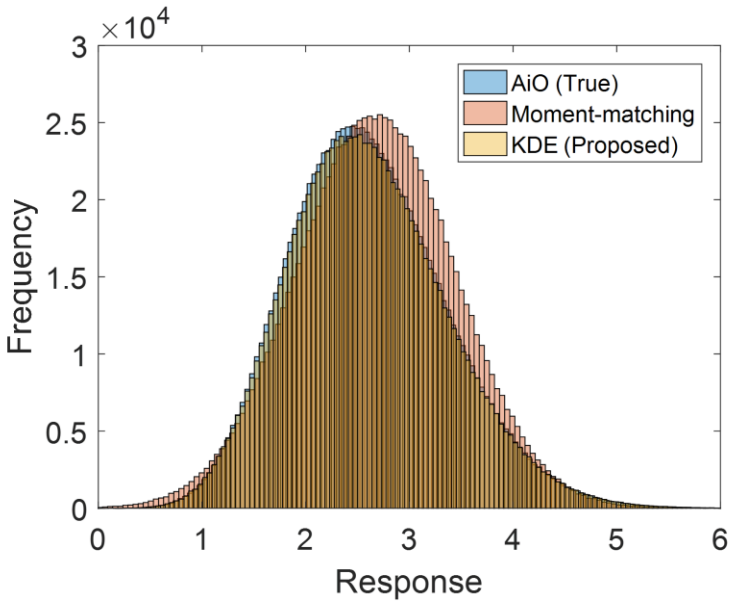

Fig. 7 Histograms of coupling response at each optimum for 3-dimensional optimization

4.2 10-dimensional Mathematical Example

In this section, a 10-dimensional mathematical example that has 6 probabilistic constraints is tested to validate the proposed PATC using multivariate KDE. The stochastic sensitivity analysis for multivariate KDE will be compared with numerical sensitivity as performed in the previous example. The whole system can be decomposed into three subsystems with one shared variable and two correlated coupling responses.

4.2.1 Formulation of Decomposed 10-dimensional Mathematical Example

The optimization of Subsystem 1 is formulated as

$$
\begin{aligned}
&\underset{\boldsymbol{\mu}_{\mathbf{X}}}{\text{minimize}} \quad \left(\mu_{X_1}\right)^{-2} + 2\left(\mu_{X_2}\right)^{2} + \left(\mu_{X_3}\right)^{2} \\
&\text{subject to} \quad \Pr[G_i(\mathbf{X}) > 0] \le 0.05 \quad \text{for } i = 1,2 \\
&\quad \text{where} \quad G_1(\mathbf{X}) = -\left(X_1^{Coup}\right)^{-2} + X_1^2 - X_2^2 - 2.5 \\
&\qquad G_2(\mathbf{X}) = X_2^2 - X_3^2 - \left(X_2^{Coup}\right)^{-2} - 2.5 \\
&\qquad X_1 \sim N(\mu_{X_1}, 0.5^2),\ X_2 \sim N(\mu_{X_2}, 0.5^2),\ X_3 \sim N(\mu_{X_3}, 0.1^2)
\end{aligned}
\tag{18}
$$

In Subsystem 1, two coupling variables are involved, and three local variables following the normal distribution are given. It is noted that the distributions of two coupling variables are estimated through multivariate KDE.

The optimization of Subsystem 2 having one shared variable and one coupling response is formulated as

$$
\begin{aligned}
&\underset{\boldsymbol{\mu}_{\mathbf{X}}}{\text{minimize}} \quad - \\
&\text{subject to} \quad \Pr[G_i(\mathbf{X}) > 0] \le 0.05 \quad \text{for } i = 3,4 \\
&\quad \text{where} \quad G_3(\mathbf{X}) = X_4^2 + X_5^{-2} - X_7^2 - 6 \\
&\qquad G_4(\mathbf{X}) = X_4^{-2} + X_6^2 - X_7^2 - 3.5 \\
&\qquad Y_1(\mathbf{X}) = \sqrt{\frac{1}{\log\left(X_4^2 + X_5^2 + X_6^2 + X_7^2\right)}} \\
&\qquad X_4 \sim N(\mu_{X_4}, 0.1^2),\ X_5 \sim N(\mu_{X_5}, 0.1^2) \\
&\qquad X_6 \sim N(\mu_{X_6}, 0.5^2),\ X_7 \sim N(\mu_{X_7}, 0.8^2)
\end{aligned}
\tag{19}
$$

In Subsystem 2, X_7 is a shared variable with Subsystem 3. Also, it has a coupling response Y_1 to be consistent with coupling variable of Subsystem 1. Note that no objective function indicates only a penalty function for augmented Lagrangian coordination is involved in promoting the consistency of linking variables.

The optimization of Subsystem 3 having one shared variable and one coupling response is formulated as

$$
\begin{aligned}
&\underset{\boldsymbol{\mu}_{\mathbf{X}}}{\text{minimize}} \quad - \\
&\text{subject to} \quad \Pr[G_i(\mathbf{X}) > 0] \le 0.05 \quad \text{for } i = 5,6 \\
&\quad \text{where} \quad G_5(\mathbf{X}) = X_7^2 + X_8^{-2} - X_9^2 - 3.5 \\
&\qquad G_6(\mathbf{X}) = X_7^{-2} + X_8^2 - X_{10}^2 - 6 \\
&\qquad Y_2(\mathbf{X}) = \sqrt{\frac{1}{\log\left(X_7^2 + X_8^2 + X_9^2 + X_{10}^2\right)}} \\
&\qquad X_7 \sim N(\mu_{X_7}, 0.8^2),\ X_8 \sim N(\mu_{X_8}, 0.1^2) \\
&\qquad X_9 \sim N(\mu_{X_9}, 0.5^2),\ X_{10} \sim N(\mu_{X_{10}}, 0.5^2)
\end{aligned}
\tag{20}
$$

Subsystem 3 has shared variable X_7 with Subsystem 2 and coupling response Y_2 as well as Subsystem 2.

Consequently, there are three subsystems and two correlated coupling variables due to a shared variable X_7 between Subsystems 2 and 3. In the following section, we can validate the stochastic sensitivity analysis for multivariate KDE using a 10-dimensional example. Note that coupling variable is not design variable in the perspective of the AiO optimization, but it is an intermediate random response to be consistent in decomposed structure.

4.2.2 Validation of Sensitivity Analysis for Multivariate Kernel Density Estimation

Firstly, the stochastic sensitivity analysis with respect to multivariate KDE has to be verified using the performance function modified from the 10-dimensional optimization. The performance function which is used can be written as

$$G(\mathbf{X}) = \left(X_1 + X_1^{Coup} \right)^2 + 2\left(X_2 + X_2^{Coup} \right)^2 - 92 \tag{21}$$

where two random variables follow a normal distribution as $N(3,0.1^2)$, and the two coupling variables are the functions of random variables which denoted as Y_1 and Y_2 in Eqs. (19) and (20) where the mean of random variables are set to 2. Thus, the two coupling variables with correlation does not follow parametric distribution unlike tests for univariate KDE. The number of samples for computing reliability is 5×10^5, and the number of samples to construct the multivariate KDE is variant, so that the numerical sensitivity for various perturbation size and proposed sensitivity analysis with respect to each mean vector are tabulated in Table 5. Since the optimal step size is dependent on various test conditions, the analytical sensitivity does not have to fit well with the numerical sensitivity of the smallest perturbation, especially in case of stochastic sensitivity. Thus, the overall trend of numerical sensitivities had become a measure to validate the developed analytical sensitivity. The proposed sensitivity analysis shows a good agreement with numerical sensitivities.

Table 5 Results of sensitivity analysis with respect to multivariate KDE

# of samples	**10 Data**		**100 Data**		**500 Data**	
Mean vector	$\mathbf{d}_1$	$\mathbf{d}_2$	$\mathbf{d}_1$	$\mathbf{d}_2$	$\mathbf{d}_1$	$\mathbf{d}_2$
FDM (5.00%)	0.2831	0.9238	0.2442	0.8250	0.2511	0.8312
FDM (1.00%)	0.1887	0.4180	0.1567	0.3530	0.1657	0.3743
FDM (0.50%)	0.1779	0.3837	0.1503	0.3189	0.1573	0.3367
FDM (0.10%)	0.1710	0.3630	0.1371	0.2940	0.1534	0.3296
FDM (0.05%)	0.1718	0.3419	0.1371	0.2813	0.1559	0.3084
Analytical sensitivity analysis	0.1682	0.3305	0.1374	0.2948	0.1436	0.2972

4.2.3 Results of Sampling-based PATC

The results of sampling-based PATC using multivariate KDE are shown in this section. Note that surrogate modeling is not employed for the sake of simplicity in this example because it is already validated in the 3-dimensional example. The normal distribution is used for uncertainty quantification in the moment-matching method, and the lower bound and upper bound for 10 design variables are given as 1 and 3. The initial design is the center of design space, and the tolerance for convergence criterion of ATC is set to 0.005. The initial Lagrange multiplier and penalty weight are 0 and 1 for all linking variables. To promote the convergence of PATC, the proportional increase ratio of penalty weight is set to 1.1 which is popular in AL-AD.

Consequently, the obvious differences in each optimum are shown in Table 6. The optimum of moment-matching induces the error since the uncertainty quantification of coupling responses is inaccurate as shown in Figure 8. In contrast, the histogram of coupling responses at the optimum computed from the proposed method has a high agreement with AiO results. It could be expectable because the uncertainty of non-normal coupling responses cannot be accurate under the scheme of moment-matching. Even if we could find other parametric distribution to represent the data well, it is still one of the parametric distributions, and the coupling response would be a nonlinear function of random variables and thus may not follow parametric distribution. Instead, the multivariate KDE that relies on the sample dataset itself facilitates the accurate uncertainty quantification along with analytical sensitivity analysis even for correlated random variables. When given samples are sparse, the moment-matching method would be better option, but we can make use of huge number of samples for

constructing KDE of coupling variables owing to surrogate model, and nonparametric density estimation such as KDE can accurately estimate underlying density function than moment-matching.

Table 6 Results of each method for 10-dimensional optimization

Method	Optimum
AiO	$[1.000, 1.972, 2.764, 1.024, 1.000, 1.000, 1.000, 1.068, 1.797, 1.000]^T$
Moment-matching	$[1.000, 1.993, 2.790, 1.022, 1.000, 1.000, 1.000, 1.198, 1.740, 1.000]^T$
KDE (Proposed)	$[1.001, 1.976, 2.769, 1.027, 1.000, 1.000, 1.000, 1.069, 1.794, 1.000]^T$

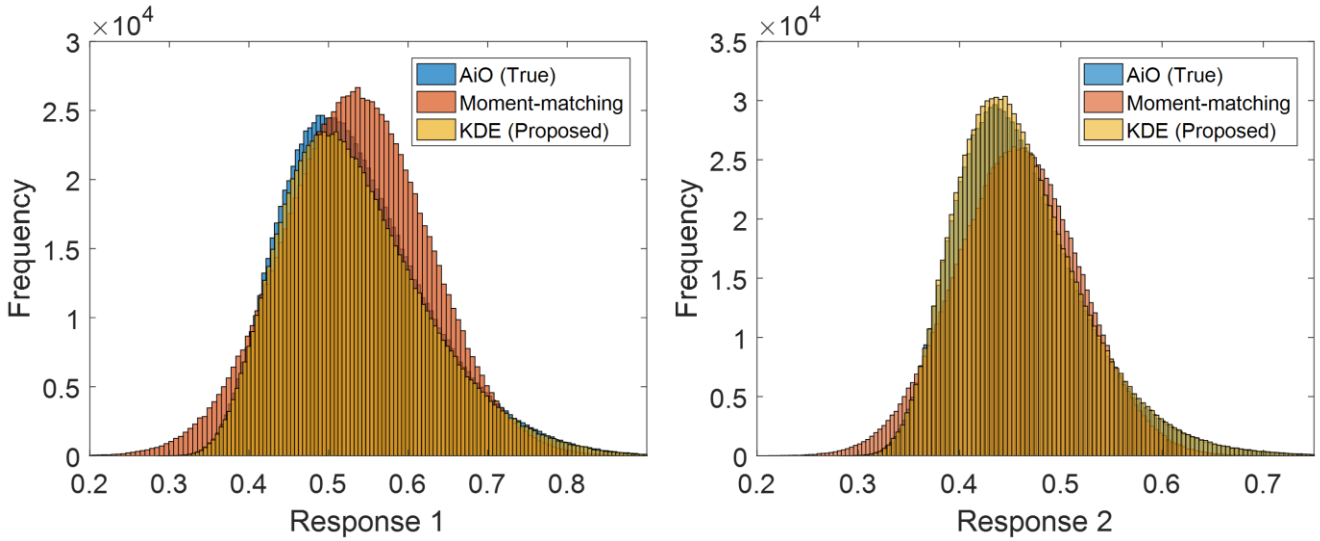

Fig. 8 Histograms of two coupling responses at each optimum for 10-dimensional optimization

5. Engineering Example: Roof Assembly Optimization

An engineering example incorporating FEA models is employed to verify feasibility of the proposed method in real complex engineering applications. This example is originated from the optimization of a bus body structure (Kang et al. 2014b) and modified by Jung et al. (2018) for the sake of simplicity. In this paper, optimization of the components − cross-sections of beams − is refined to increase the number of design variables. There is a roof assembly optimization to satisfy displacement and von Mises stress constraints with respect to the bending and torsion as shown in Figure 9 (a). On the other hand, the roof assembly consists of various types of

beams among them two types of I-beams used in the roof assembly shown in Figure 9 (b) are selected for optimization. Thus, there are six random design variables in each cross-section of the beam, and linking variables are the cross-sectional area and two perpendicular moments of inertia (MOI) of the cross-section. In the roof optimization, the objective function is a penalty function for consistency constraints, and design variables are coupling variables that are the area and MOI linked with each beam without any local and shared variable. In the optimization of beam, the objective function is mass of beam and penalty function for consistency constraints, and there are only local variables to be optimized.

The decomposed structure is shown with three subsystems where the objective is to reduce the mass only with constraints described in Figure 10, and it shows local design variables, objective function, inequality constraint functions, and equality constraint function from top to bottom in each box. The first subsystem on the top level denoted as roof assembly in Figure 10 has a FEA model for the roof, so that the maximum displacements and stresses under two types of loading can be computed for the individual RBDO of the roof assembly. Note that maximum stress is defined as the von Mises stress on specific nodes where the maximum stress is frequently observed. On the other hand, two subsystems for the beam are located in the bottom level. It has coupling responses such as area and MOI, but it is able to be calculated by a simple mathematical expression. Thus, the FEA model is not required in subsystems for the beam. Briefly, a single FEA model for roof assembly is used to compute the limit-state function, and the coupling responses of the beam can be easily obtained without FEA model.

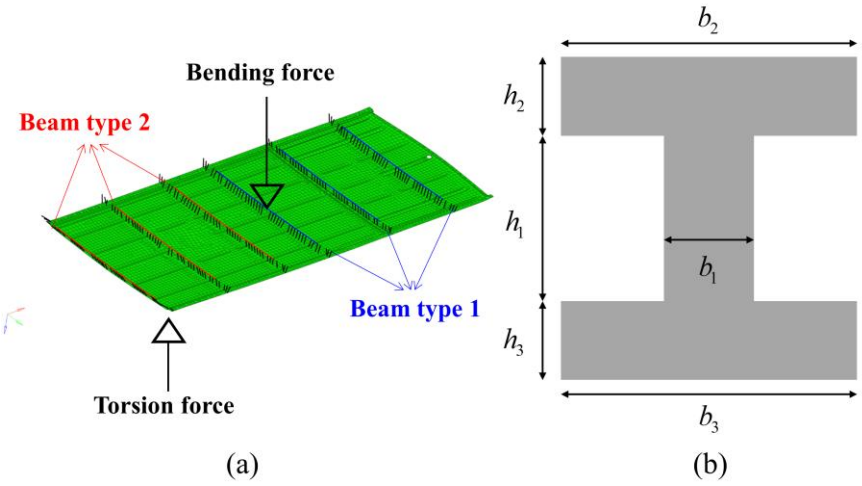

Fig. 9 (a) FEA model of a roof assembly including various beams and (b) design variables in the cross-section of I-beam

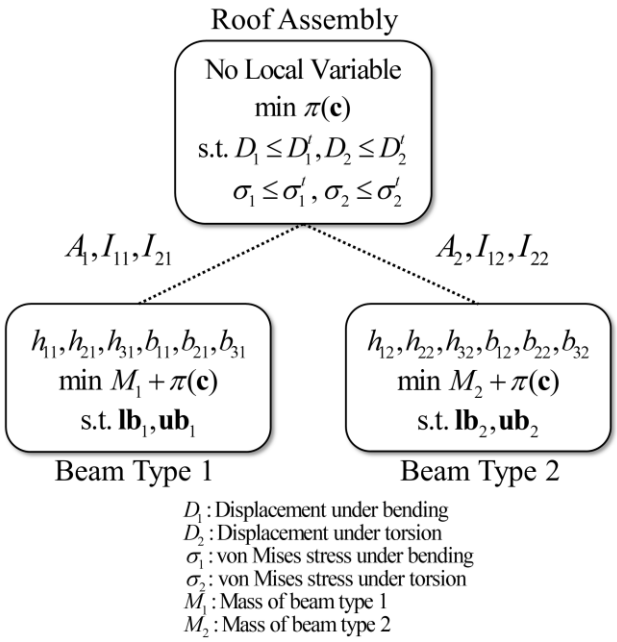

Fig. 10 Decomposition details for a roof assembly optimization with two types of beams

In conclusion, the original 12-dimensional RBDO problem is divided into three 6-dimensional RBDO problems linked with coupling variables. For a roof assembly, there are 6 coupling variables which are MOI of

each beam, and the maximum allowable displacements and stresses when a single force is exerted on the center of the structure (i.e., bending) and the given boundary node (i.e., torsion) are set to 75.00 mm, 442.78 mm, 334.30 MPa, and 403.66 MPa, respectively. The target probability of failure is set to 5.00% for each constraint. The design space is defined in ±20% from the initial design variable. On the other hand, 6 design variables in each beam follow a normal distribution where the coefficient of variation is set to 0.01. Especially, in component-level optimization (i.e., beam optimization), the surrogate modeling is unnecessary since the coupling responses which are MOI of the cross-section can be computed in simple mathematical functions without FEA model. On the other hand, in assembly-level optimization (i.e., roof assembly optimization), the FEA model of a roof assembly is used to obtain displacements and stresses. Latin hypercube sampling (LHS) is used for 150 initial samplings in 6-dimensional design space of the roof assembly. The normalized mean squared error (NMSE) of leave-one-out cross-validation (LOOCV) is used to quantify the accuracy of the surrogate model and its stopping tolerance is set to 0.005. There are 4 surrogate models in roof assembly which are the displacement and von Mises stress under bending and torsion, and maximum NMSE is 0.0026 among 4 surrogate models. Thus, the surrogate model can be thought as accurate.

Table 7 shows roof assembly optimization results by deterministic ATC and the proposed PATC. The deterministic ATC reduced the roof assembly mass by 15% satisfying four displacement and stress constraints. Using the deterministic optimum as the initial design, the sampling-based PATC is performed to satisfy 95% reliability of four displacement and stress constraints. From the table, it can be seen that the displacement constraint for torsion and von Mises stress constraints for bending and torsion are active in deterministic ATC and the normalized mass is increased from 0.850 to 0.861 to guarantee reliability. This engineering example verifies the feasibility of the proposed sampling-based PATC.

Table 7 Roof assembly optimization results by deterministic ATC and proposed PATC

	Initial	Deterministic	Proposed PATC
Roof assembly			
Normalized mass	1.000	0.850	0.861

Displacement for bending [mm]	73.874	74.285	74.129
Displacement for torsion [mm]	440.704	442.773	442.349
von Mises stress for bending [MPa]	334.510	334.291	334.090
von Mises stress for torsion [MPa]	405.750	403.658	403.563
1st type beam			
h_1 [mm]	10.000	11.617	11.642
h_2 [mm]	5.000	4.000	4.034
h_3 [mm]	5.000	4.000	4.025
b_1 [mm]	5.000	4.000	4.007
b_2 [mm]	15.000	17.517	17.929
b_3 [mm]	15.000	12.000	12.093
2nd type beam			
h_1 [mm]	10.000	9.013	8.991
h_2 [mm]	5.000	4.000	4.053
h_3 [mm]	5.000	4.000	4.056
b_1 [mm]	5.000	4.000	4.014
b_2 [mm]	15.000	17.358	17.645
b_3 [mm]	15.000	18.000	17.695

6. Conclusion

This paper proposes sampling-based PATC using multivariate KDE for uncertainty propagation between linked subsystems. The uncertainty propagation of linking variables – essential process to attain the consistency – is developed to deliver statistical information between linked subsystems utilizing KDE, unlike existing methods which use only statistical moments and assumed parametric distribution. Through the proposed method, individual optimization of subsystems incorporating uncertainty can yield a reliable optimum efficiently under the scheme of sampling-based RBDO, and uncertainty of correlated coupling variables sharing the same source of uncertainty has been successfully treated employing stochastic sensitivity analysis for multivariate KDE. It means that the coupling variables propagated from linked subsystems behave as random design variables through multivariate KDE and stochastic sensitivity analysis at the current design point. The proposed method is successfully applied to real engineering problems incorporating FEA, and thus it is desirable to use surrogate models since PATC requires a large number of function evaluations with iterative optimizations. In this paper, a sequential sampling strategy for constructing Kriging model is used due to the practical issue, but any types of improved strategies for sampling and surrogate model can be implemented.

In future work, the dimension reduction effect of the proposed ATC will be further investigated. In previous works, it may be impractical to combine all subsystems into one due to complexity in existing ATC researches, and thus AiO is used only for comparison of accuracy rather than efficiency. However, a decomposed structure inherently contains several subsystems with reduced dimension which implies that the number of samples for accurate surrogate modeling may decrease in the ATC framework compared with the high-dimensional AiO system. Hence, it will be further studied how to develop efficient surrogate modeling based on the ATC framework which can be applied to solve large-scale & high dimensional engineering optimization problems by avoiding the curse of dimensionality.

7. Acknowledgements

This research was supported by the development of thermoelectric power generation system and business model utilizing non-use heat of industry funded by the Korea Institute of Energy Technology Evaluation and Planning (KETEP) and the Ministry of Trade Industry & Energy (MOTIE) of the Republic of Korea (No. 20172010000830) and the National Research Foundation of Korea (NRF) grant funded by the Korean government (NRF-2017R1C1B2005266).

8. Replication of Results

Matlab codes for the 3-dimensional and 10-dimensional mathematical examples in Section 4 are uploaded on https://github.com/Yongsu-Jung/SMO_PATC.git. Unfortunately, the engineering optimization is related to FEA models that are restricted so that it cannot be shared. Overall concepts and algorithms can be validated through the mathematical example.

9. Reference

Adhikari, S. (2004). Reliability analysis using parabolic failure surface approximation. *Journal of Engineering Mechanics*, 130(12), 1407-1427.

Alexandrov, N. M., & Lewis, R. M. (2002). Analytical and computational aspects of collaborative optimization for multidisciplinary design. *AIAA Journal*, 40(2), 301-309.

Allison, J. T., Kokkolaras, M., & Papalambros, P. Y. (2009). Optimal partitioning and coordination decisions in decomposition-based design optimization. *Journal of Mechanical Design*, 131(8), 081008.

Bae, S., Kim, N. H., & Jang, S. G. (2018). Reliability-based design optimization under sampling uncertainty: shifting design versus shaping uncertainty. *Structural and Multidisciplinary Optimization*, 57(5), 1845-1855.

Bayrak, A. E., Kang, N., & Papalambros, P. Y. (2016). Decomposition-based design optimization of hybrid electric powertrain architectures: Simultaneous configuration and sizing design. *Journal of Mechanical Design*, 138(7), 071405.

Chen, Y. C. (2017). A tutorial on kernel density estimation and recent advances. *Biostatistics & Epidemiology*, 1(1), 161-187.

Chen, Z., Qiu, H., Gao, L., Li, X., & Li, P. (2014). A local adaptive sampling method for reliability-based design optimization using Kriging model. *Structural and Multidisciplinary Optimization*, 49(3), 401-416.

Cho, H., Choi, K. K., Lee, I., & Lamb, D. (2016). Design sensitivity method for sampling-based RBDO with varying standard deviation. *Journal of Mechanical Design*, 138(1), 011405.

Cho, S. G., Jang, J., Kim, S., Park, S., Lee, T. H., Lee, M., ... & Hong, S. (2016). Nonparametric approach for uncertainty-based multidisciplinary design optimization considering limited data. *Structural and Multidisciplinary Optimization*, 54(6), 1671-1688.

Denny, M. (2001). Introduction to importance sampling in rare-event simulations. *European Journal of Physics*, 22(4), 403.

Du, X., & Chen, W. (2001). A most probable point-based method for efficient uncertainty analysis. Journal of Design and Manufacturing automation, 4(1), 47-66.

Dubourg, V., Sudret, B., & Bourinet, J. M. (2011). Reliability-based design optimization using kriging surrogates and subset simulation. *Structural and Multidisciplinary Optimization*, 44(5), 673-690.

Han, J., & Papalambros, P. Y. (2010). A sequential linear programming coordination algorithm for analytical target cascading. *Journal of Mechanical Design*, 132(2), 021003.

Jung, Y., Kang, N., & Lee, I. (2018). Modified augmented Lagrangian coordination and alternating direction method of multipliers with parallelization in non-hierarchical analytical target cascading. *Structural and Multidisciplinary Optimization*, 58(2), 555-573.

Jung, Y., Cho, H., & Lee, I. (2019). MPP-based approximated DRM (ADRM) using simplified bivariate approximation with linear regression. *Structural and Multidisciplinary Optimization*, *59*(5), 1761-1773.

Kang, N., Kokkolaras, M., & Papalambros, P. Y. (2014a). Solving multiobjective optimization problems using quasi-separable MDO formulations and analytical target cascading. *Structural and Multidisciplinary Optimization*, 50(5), 849-859.

Kang, N., Kokkolaras, M., Papalambros, P. Y., Yoo, S., Na, W., Park, J., & Featherman, D. (2014b). Optimal design of commercial vehicle systems using analytical target cascading. *Structural and Multidisciplinary Optimization*, 50(6), 1103-1114.

Kang, K., Qin, C., Lee, B., & Lee, I. (2019). Modified screening-based Kriging method with cross validation and application to engineering design. *Applied Mathematical Modelling*, *70*, 626-642.

Kim, H. M., Rideout, D. G., Papalambros, P. Y., & Stein, J. L. (2003). Analytical target cascading in automotive vehicle design. *Journal of Mechanical Design*, 125(3), 481-489.

Kim, H. M., Chen, W., & Wiecek, M. M. (2006). Lagrangian coordination for enhancing the convergence of analytical target cascading. *AIAA Journal*, 44(10), 2197-2207.

Kokkolaras, M., Louca, L., Delagrammatikas, G., Michelena, N., Filipi, Z., Papalambros, P., ... & Assanis, D. (2004). Simulation-based optimal design of heavy trucks by model-based decomposition: An extensive analytical target cascading case study. *International Journal of Heavy Vehicle Systems*, 11(3-4), 403-433.

Kokkolaras, M., Mourelatos, Z. P., & Papalambros, P. Y. (2006). Design optimization of hierarchically decomposed multilevel systems under uncertainty. *Journal of Mechanical Design*, 128(2), 503-508.

Lee, I., Choi, K. K., Noh, Y., Zhao, L., & Gorsich, D. (2011). Sampling-based stochastic sensitivity analysis using score functions for RBDO problems with correlated random variables. *Journal of Mechanical Design*, 133(2), 021003.

Lee, I., Noh, Y., & Yoo, D. (2012). A novel second-order reliability method (SORM) using noncentral or generalized chi-squared distributions. *Journal of Mechanical Design*, 134(10), 100912.

Lee, T. H., & Jung, J. J. (2008). A sampling technique enhancing accuracy and efficiency of metamodel-based RBDO: Constraint boundary sampling. *Computers & Structures*, 86(13), 1463-1476.

Lim, J., Lee, B., & Lee, I. (2014). Second-order reliability method-based inverse reliability analysis using Hessian update for accurate and efficient reliability-based design optimization. *International Journal for Numerical Methods in Engineering*, 100(10), 773-792.

Liu, H., Chen, W., Kokkolaras, M., Papalambros, P. Y., & Kim, H. M. (2006). Probabilistic analytical target cascading: a moment matching formulation for multilevel optimization under uncertainty. *Journal of Mechanical Design*, 128(4), 991-1000.

Martins, J. R., & Lambe, A. B. (2013). Multidisciplinary design optimization: a survey of architectures. *AIAA Journal*, 51(9), 2049-2075.

Michelena, N., Park, H., & Papalambros, P. Y. (2003). Convergence properties of analytical target cascading. *AIAA Journal*, 41(5), 897-905.

Ouyang, Q., Chen, X., & Yao, W. (2014). Sequential probabilistic analytical target cascading method for hierarchical multilevel optimization under uncertainty. *Structural and Multidisciplinary Optimization*, 49(2), 267-280.

Ouyang, Q., Yao, W., & Chen, X. (2018). Mixed uncertainty based analytical target cascading: an approach for hierarchical multilevel optimization under probabilistic and interval mixed uncertainties. *Structural and Multidisciplinary Optimization*, 57(4), 1475-1493.

Papalambros, P. Y., & Wilde, D. J. (2017). Principles of optimal design: modeling and computation. *Cambridge university press.*

Rubinstein, R. Y., & Kroese, D. P. (2016). Simulation and the Monte Carlo method (Vol. 10). *John Wiley & Sons.*

Silverman, B. W. (2018). Density estimation for statistics and data analysis. *Routledge.*

Tosserams, S., Etman, L. F. P., Papalambros, P. Y., & Rooda, J. E. (2006). An augmented Lagrangian relaxation for analytical target cascading using the alternating direction method of multipliers. *Structural and Multidisciplinary Optimization*, 31(3), 176-189.

Tosserams, S., Etman, L. F. P., & Rooda, J. E. (2008). Augmented Lagrangian coordination for distributed optimal design in MDO. *International Journal for Numerical Methods in Engineering*, 73(13), 1885-1910.

Tosserams, S., Kokkolaras, M., Etman, L. F. P., & Rooda, J. E. (2010). A nonhierarchical formulation of analytical target cascading. *Journal of Mechanical Design*, 132(5), 051002.

Tu, J., Choi, K. K., & Park, Y. H. (1999). A new study on reliability-based design optimization. *Journal of Mechanical Design*, 121(4), 557-564.

Xiong, F., Yin, X., Chen, W., & Yang, S. (2010). Enhanced probabilistic analytical target cascading with application to multi-scale design. *Engineering Optimization*, 42(6), 581-592.

Yao, W., Chen, X., Luo, W., van Tooren, M., & Guo, J. (2011). Review of uncertainty-based multidisciplinary design optimization methods for aerospace vehicles. *Progress in Aerospace Sciences*, 47(6), 450-479.